Article

Rifamycin W Analogues from *Amycolatopsis mediterranei* S699 Δ*rif*-*orf*5 Strain

Yanrong Shi [1,2], **Feng Ye** [1], **Yuliang Song** [1], **Xiaochun Zhang** [1], **Chunhua Lu** [1] **and Yuemao Shen** [1,*]

[1] Key Laboratory of Chemical Biology (Ministry of Education), School of Pharmaceutical Sciences, Cheeloo College of Medicine, Shandong University, Jinan 250012, China; yrshi910212@sdu.edu.cn (Y.S.); yefeng1997@mail.sdu.edu.cn (F.Y.); 201936124@mail.sdu.edu.cn (Y.S.); 201816082@mail.sdu.edu.cn (X.Z.); ahua0966@sdu.edu.cn (C.L.)

[2] Key Laboratory Experimental Teratology of the Ministry of Education, Department of Physiology, School of Basic Medical Sciences, Cheeloo College of Medicine, Shandong University, Jinan 250012, China

[*] Correspondence: yshen@sdu.edu.cn; Tel.: +86-531-8838-2108

Abstract: Rifamycin W, the most predominant intermediate in the biosynthesis of rifamycin, needs to undergo polyketide backbone rearrangement to produce rifamycin B via an oxidative cleavage of the C-12/C-29 double bond. However, the mechanism of this putative oxidative cleavage has not been characterized yet. Rif-Orf5 (a putative cytochrome P450 monooxygenase) was proposed to be involved in the cleavage of this olefinic moiety of rifamycin W. In this study, the mutant strain *Amycolatopsis mediterranei* S699 Δ*rif-orf5* was constructed by in-frame deleting the *rif-orf5* gene to afford thirteen rifamycin W congeners (**1–13**) including seven new ones (**1–7**). Their structures were elucidated by extensive analysis of 1D and 2D NMR spectroscopic data and high-resolution ESI mass spectra. Presumably, compounds **1–4** were derivatized from rifamycin W via C-5/C-11 retro-Claisen cleavage, and compounds **1–3**, **9** and **10** featured a hemiacetal. Compounds **5–7** and **11** showed oxygenations at various sites of the *ansa* chain. In addition, compounds **1–3** exhibited antibacterial activity against *Staphylococcus aureus* with minimal inhibitory concentration (MIC) values of 5, 40 and 0.5 µg/mL, respectively. Compounds **1** and **3** showed modest antiproliferative activity against HeLa and Caco-2 cells with half maximal inhibitory concentration (IC$_{50}$) values of about 50 µM.

Keywords: *Amycolatopsis mediterranei* S699; rifamycin W; polyketide backbone rearrangement; oxidative cleavage

1. Introduction

Ansamycins are a family of macrolactam antibiotics that are synthesized by type I polyketide synthase (PKS), which are structurally characterized by an aromatic moiety bridged at nonadjacent positions by an aliphatic chain (*ansa* chain) [1,2]. As the representative members of the ansamycin family, rifamycins were first isolated from *Amycolatopsis mediterranei* S699 in 1957 [3–5]. Semi-synthetic rifamycin derivatives, such as rifampicin, rifapentine and rifambutin, have long been the first-line antituberculosis drugs since the mid-1960s, and are effective in combating leprosy and tuberculosis involved in AIDS-related mycobacterial infections [6–9]. However, *Mycobacterium tuberculosis* has developed significantly increased resistance to rifamycin antibiotics due to their extensive clinical use during recent decades [10,11].

The biosynthesis of rifamycins has been continuously studied since the 1980s, which can be divided into three stages. During the first two stages, the biosynthesis of start unit 3-amino-5-hydroxybenzoic acid (AHBA) and the polyketide skeleton were investigated, respectively. The third stage is still in progress, involving exploring hypotheses concerning post-PKS modifications [12–16]. As the most predominant intermediate in rifamycin biosynthesis, rifamycin W must undergo C-12/C-29 double bond oxidative cleavage to form 27-*O*-demethyl-25-*O*-deacetyl-rifamycin S (DMDARS) that is the basic rifamycin B

polyketide skeleton. However, the mechanism of this putative oxidative cleavage has not been characterized yet [16,17].

In this study, a candidate cytochrome P450 oxidase gene, *rif-orf5*, which may be responsible for the oxidative cleavage of the rifamycin W *ansa* chain, was inactivated in *A. mediterranei* S699. The mutant strain *A. mediterranei* S699 Δ*rif-orf5* cultivated for 7 d on YMG agar medium resulted in the isolation of thirteen rifamycin W congeners (**1–13**) including seven new ones (**1–7**) (Figure 1).
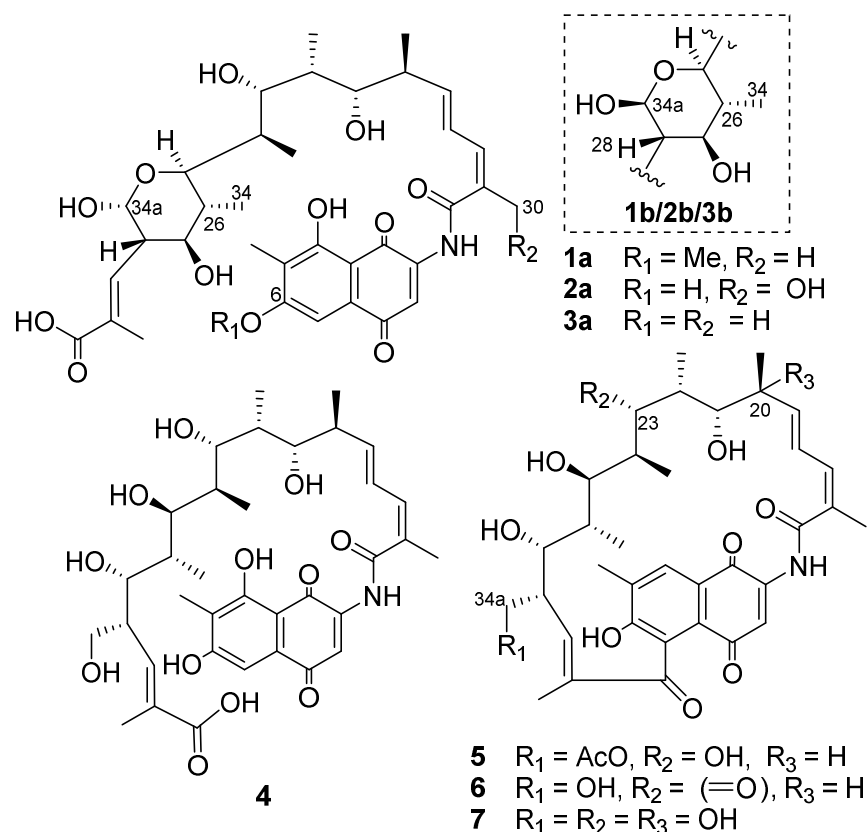
Figure 1. Structures of rifamycin W congeners **1–7**.

2. Materials and Methods

2.1. Bacterial Strains, Plasmids and Culture Media

The *Amycolatopsis mediterranei* S699 strain, isolated in 1957 in St. Raphael, France [5], was stored in our lab. The *A. mediterranei* S699 Δ*rif-orf5* strain was constructed by deleting the *rif-orf5* gene through homologous recombination. The *A. mediterranei* S699 Δ*rif-orf5::orf5* strain was constructed by transformation of the *rif-orf5* gene into the Δ*rif-orf5* mutant through electroporation. These strains were grown on YMG (yeast extract 4 g, malt extract 10 g, glucose 4 g, 20 g agar, ddH$_2$O 1000 mL, pH 7.2) agar media at 28 °C for the production of rifamycins.

The *Escherichia coli* DH5α strain was used for plasmid propagation. Suicide vector pOJ260 was used for gene knock-out. Integrating vector pSET152 was used for gene complementation [18]. *E. coli* strains were maintained in LB (tryptone 10 g, yeast extract 5 g, NaCl 10 g, ddH$_2$O 1000 mL, pH 7.2) media at 37 °C. Apramycin was added into media at a final concentration of 50 μg·mL^{-1}. Cells were stocked with 20% glycerol and stored at −80 °C.

2.2. Molecular Cloning and Mutant Construction

2.2.1. Construction of the *rif-orf5* Gene Knock-Out Mutant Δ*rif-orf5*

First, the *rif-orf5* gene knock-out vector pOJ260-orf5 was constructed. Two ca. 2 kb DNA fragments flanking upstream and downstream of the target gene were amplified from the genomic DNA of *A. mediterranei* S699, and named HF1 and HF2, respectively. The purified homologous fragments HF1 and HF2 were digested with HindIII/XbaI and XbaI/EcoRI, and cloned into linearized HindIII/EcoRI digested pOJ260. The ligation product was transformed into DH5α-competent cells. Positive clones were verified by restriction enzyme digestion and sequencing (Figures S1A and S2). The gene knock-out vector pOJ260-orf5 was introduced into the rifamycin-producing strain *A. mediterranei* S699 by electrotransformation [19]. Apramycin-resistant (AprR) colonies were selected and confirmed to be single cross-over mutants by PCR amplification (Figures S1B and S3A). Apramycin-sensitive (AprS) colonies were counterselected from the initial AprR single cross-over colonies after several rounds of nonselective growth, and confirmed to be double cross-over gene knock-out mutant Δ*rif-orf5* by PCR amplification (Figures S1B and S3B).

2.2.2. Construction of the *rif-orf5* Gene Complementation Mutant Δ*rif-orf5::orf5*

First, the *rif-orf5* gene complementation vector pSET152-orf5 was constructed. The targeted gene *rif-orf5* was amplified using the genomic DNA of *A. mediterranei* S699 as a template. The purified PCR fragment was digested with NdeI and XbaI, and cloned into the downstream of the *rif*Kp promoter in pSET152 through Gibson assembly [20]. Similarly, the assembled product was transformed into DH5α-competent cells, and positive clones were verified by restriction enzyme digestion and sequencing (Figure S4). The gene complementation vector pSET152-orf5 was transformed into the *rif-orf5* gene knock-out mutant Δ*rif-orf5* by electroporation. Apramycin-sensitive (AprS) colonies were selected and confirmed to be the *rif-orf5* gene complementation mutant Δ*rif-orf5::orf5* by PCR amplification (Figure S5).

Primers used in this study are shown in Table S1.

2.3. HPLC Detection of the Metabolites in Mutants

A. mediterranei S699 mutants were inoculated on YMG agar media (100 mL) and cultivated for 7 days at 28 °C. The culture was diced and extracted overnight with EtOAc at room temperature. The concentrated crude extract was dissolved in 1 mL MeOH, and analyzed by high-pressure liquid chromatography (HPLC; Agilent 1200, Santa Clara, CA, USA) in a gradient system consisting of ddH_2O + 0.5% formic acid as solvent A and acetonitrile as solvent B. The program of solvent gradient was as follows: 20–35% B in the first 5 min, 35–55% B from 5 to 19 min, 55–65% B from 19 to 23 min, 65–100% B from 23 to 27 min. Flow rate was 1 mL/min, and UV detection was monitored at 254 nm (Figure S6).

2.4. Extraction and Isolation of the Metabolites from the Δ*rif-orf5* Strain

2.4.1. General Experimental Procedures

The nuclear magnetic resonance (NMR) spectra were recorded on Bruker 400 MHz NMR spectrometer. HRESIMS analyses were carried out on an LTQ-Orbitrap XL (Thermo Scientific, Waltham, MA, USA). HPLC was performed on an Agilent 1200. Semi-preparative HPLC was performed on a Waters 1525 Binary HPLC Pump (Agilent Eclipse XDB-C_{18}, 5 µm, 9.4 × 250 mm) with a Waters 996 Photodiode Array Detector (Milford, MA, USA). Sephadex LH-20 was obtained from GE Amersham Biosciences (Piscataway, NJ, USA). Column chromatography (CC) was performed over reversed-phase (RP) C_{18} silica gel (Merck, Darmstadt, Germany). Silica gel GF_{254} for thin-layer chromatography (TLC) was purchased from Qingdao Marine Chemical Ltd. (Qingdao, China). Optical rotations were measured on an Auton Paar MCP200 Automatic Polarimeter. IR spectra (KBr) were obtained on a Thermo Fisher Scientific Nicolet 6700 FT-IR spectrometer (Waltham, MA, USA). Compounds were visualized under UV light and by iodine vapor.

2.4.2. Fermentation, Extraction and Isolation of the Metabolites from the Δ*rif-orf5* Strain

The fermentation (20 L) was performed on YMG agar Petri dishes for 7 d at 28 °C. The culture was diced and extracted overnight with EtOAc/MeOH (4:1, *v/v*) at room temperature three times. The crude extract was partitioned between H_2O and EtOAc (1:1, *v/v*) until the H_2O layer was colorless. The EtOAc extract was partitioned between 95% aqueous MeOH and petroleum ether (PE) to afford the defatted MeOH extract. The MeOH extract was fractionated by medium-pressure liquid chromatography (MPLC) over RP C_{18} silica gel (130 g) eluted with gradient aqueous CH_3CN (30%, 50%, 70% and 100% CH_3CN, 500 mL each) to give Fr. A–J.

Fr. C (1.43 g) was purified by HPLC (4 mL/min, UV 254 nm) eluted with 32% CH_3CN to afford **7** (t_R 13.4 min, 17.5 mg) and **12** (t_R 6.2 min, 29.8 mg). Fr. D (5.62 g) was subjected to CC over silica gel (150 g) eluted with gradient CH_2Cl_2:MeOH (50:1, 30:1, 15:1 and 5:1, 500 mL each) to afford Fr. D1–4. Fr. D2 (1.85 g) was purified by HPLC (4 mL/min, UV 254 nm) eluted with 35% CH_3CN to afford **10** (t_R 8.6 min, 33 mg) and **14** (t_R 10.3 min, 41 mg). Fr. D3 (2.49 g) was purified by HPLC (4 mL/min, UV 254 nm) eluted with 40% CH_3CN to afford **6** (t_R 7.9 min, 9.9 mg), **8** (t_R 15.3 min, 17.0 mg) and **13** (t_R 11.4 min, 179.5 mg). Fr. E (1.74 g) was purified by HPLC (4 mL/min, UV 254 nm) eluted with 43% CH_3CN to afford **2** (t_R 7.5 min, 10.5 mg), **4** (t_R 13.4 min, 6.8 mg) and **5** (t_R 6.2 min, 29.7 mg). Similarly, compounds **9** (12.3 mg) and **11** (7.2 mg) were obtained from Fr. F, and **3** (13.5 mg) was purified from Fr. G by HPLC (4 mL/min, UV 254 nm) eluted with 45% CH_3CN. Fr. I gave compound **1** (6.6 mg) through HPLC (4 mL/min; UV 254 nm) eluted with 58% CH_3CN.

Compound **1**: dark brown powder; $[\alpha]^{20}_D$ = +10.0 (*c* 0.10, MeOH); UV (MeOH) λ_{max} (logε) 217 (4.40), 269 (4.30), 325 (4.00) nm; IR (KBr) ν_{max} 3369, 2963, 2925, 1688, 1631, 1496, 1322, 1142, 977, 862 cm^{-1}; ^{1}H NMR data, Table 1; ^{13}C NMR data, Table 2; HRESIMS: *m/z* 686.3172 [M + H]$^+$ (calcd for $C_{36}H_{48}NO_{12}^+$, 686.3171), and 708.2992 [M + Na]$^+$ (calcd for $C_{36}H_{47}NNaO_{12}^+$, 708.2990).

Compound **2**: dark brown powder; $[\alpha]^{20}_D$ = −4.0 (*c* 0.10, MeOH); UV (MeOH) λ_{max} (logε) 218 (4.38), 274 (4.27), 323 (3.99) nm; IR (KBr) ν_{max} 3359, 2972, 2931, 1687, 1629, 1503, 1326, 1122, 1047, 979, 875, 755 cm^{-1}; ^{1}H NMR data, Table 1; ^{13}C NMR data, Table 2; HRESIMS: *m/z* 688.2956 [M + H]$^+$ (calcd for $C_{35}H_{46}NO_{13}^+$, 688.2964) and 710.2781 [M + Na]$^+$ (calad for $C_{35}H_{45}NNaO_{13}^+$, 710.2783).

Compound **3**: dark brown powder; $[\alpha]^{20}_D$ = +12.0 (*c* 0.10, MeOH); UV (MeOH) λ_{max} (logε) 218 (4.12), 272 (3.94), 323 (3.66) nm; IR (KBr) ν_{max} 3366, 2972, 2932, 1598, 1498, 1377, 1325, 1121, 1069, 981, 758 cm^{-1}; ^{1}H NMR data, Table 1; ^{13}C NMR data, Table 2; HRESIMS: *m/z* 672.3011 [M + H]$^+$ (calcd for $C_{35}H_{46}NO_{12}^+$, 672.3015), and 694.2835 [M + Na]$^+$ (calcd for $C_{35}H_{45}NNaO_{12}^+$, 694.2834).

Compound **4**: maroon powder; $[\alpha]^{20}_D$ = +28.0 (*c* 0.10, MeOH); UV (MeOH) λ_{max} (logε) 214 (3.90), 273 (3.66), 323 (3.37) nm; IR (KBr) ν_{max} 3409, 2948, 2836, 1656, 1451, 1413, 1203, 1114, 1024, 695 cm^{-1}; ^{1}H NMR data, Table 3; ^{13}C NMR data, Table 2; HRESIMS: *m/z* 674.3172 [M + H]$^+$ (calcd for $C_{35}H_{48}NO_{12}^+$, 674.3171), and 696.2988 [M + Na]$^+$ (calcd for $C_{35}H_{47}NNaO_{12}^+$, 696.2990).

Compound **5**: brown powder; $[\alpha]^{20}_D$ = +206.3 (*c* 0.10, MeOH); UV (MeOH) λ_{max} (logε) 225 (4.44), 263 (4.24), 326 (3.93) nm; IR (KBr) ν_{max} 3368, 2970, 2934, 1631, 1607, 1495, 1388, 1197, 1053, 974, 887 cm^{-1}; ^{1}H NMR data, Table 3; ^{13}C NMR data, Table 2; HRESIMS: *m/z* 698.3170 [M + H]$^+$ (calcd for $C_{37}H_{48}NO_{12}^+$, 698.3171), and 720.2986 [M + Na]$^+$ (calcd for $C_{37}H_{47}NNaO_{12}^+$, 720.2990).

Compound **6**: brown powder; $[\alpha]^{20}_D$ = +174.2 (*c* 0.10, MeOH); UV (MeOH) λ_{max} (logε) 222 (4.42), 312 (3.91) nm; IR (KBr) ν_{max} 3347, 2972, 2932, 1629, 1495, 1387, 1323, 1196, 968, 884 cm^{-1}; ^{1}H NMR data, Table 3; ^{13}C NMR data, Table 2; HRESIMS: *m/z* 654.2914 [M + H]$^+$ (calcd for $C_{35}H_{44}NO_{11}^+$, 654.2909), and 676.2731 [M + Na]$^+$ (calcd for $C_{35}H_{48}NNaO_{11}^+$, 676.2728).

Compound **7**: brown powder; $[\alpha]^{20}_D$ = +246.3 (*c* 0.11, MeOH); UV (MeOH) λ_{max} (logε) 222 (4.38), 319 (3.89) nm; IR (KBr) ν_{max} 3362, 2967, 2935, 1631, 1497, 1389, 1318, 1193, 1054, 976, 801 cm^{-1}; ^{1}H NMR data, Table 3; ^{13}C NMR data, Table 2; HRESIMS: *m/z* 672.3019 [M +

H]$^+$ (calcd for C$_{35}$H$_{46}$NO$_{12}$$^+$, 672.3015), and 694.2839 [M + Na]$^+$ (calcd for C$_{35}$H$_{45}$NNaO$_{12}$$^+$, 694.2834).

Table 1. ^{1}H NMR spectroscopic data (400 MHz, CD$_3$OD) of compounds **1**–**3** (δ_H, J in Hz) *.

| Position | 1 | | 2 | | 3 | |
	1a	1b	2a	2b	3a	3b
3	7.64 (s)	7.64 (s)	7.64 (s)	7.64 (s)	7.61 (s)	7.61 (s)
5	7.18 (s)	7.18 (s)	6.99 (s)	6.99 (s)	7.02 (s)	7.02 (s)
MeO-6	4.00 (s)	4.00 (s)				
13	1.89 (s)	1.87 (s)	1.90 (s)	1.88 (s)	1.90 (s)	1.88 (s)
14	2.09 (s)	2.09 (s)	2.07 (s)	2.07 (s)	2.09 (s)	2.09 (s)
17	6.50 (d, 10.8)	6.50 (d, 10.8)	6.64 (d, 11.3)	6.64 (d, 11.3)	6.50 (d, 10.8)	6.50 (d, 10.8)
18	6.87 (dd, 11.2, 14.9)	6.87 (dd, 11.2, 14.9)	7.21 (dd, 11.1, 15.0)	7.21 (dd, 11.1, 15.0)	6.86 (dd, 12.4, 14.9)	6.86 (dd, 12.4, 14.9)
19	6.08 (m)	6.08 (m)	6.23 (m)	6.23 (m)	6.07 (m)	6.07 (m)
20	2.44 (m)	2.44 (m)	2.52 (m)	2.52 (m)	2.47 (m)	2.47 (m)
21	3.82 (m)	3.82 (m)	3.84 (d, 8.7)	3.84 (d, 8.7)	3.83 (m)	3.83 (m)
22	2.04 (m)	2.04 (m)	1.95 (m)	1.95 (m)	1.96 (m)	1.96 (m)
23	3.62 (m)	3.62 (m)	3.64 (m)	3.64 (m)	3.62 (m)	3.62 (m)
24	1.98 (m)	1.98 (m)	2.03 (m)	2.03 (m)	2.02 (m)	2.02 (m)
25	3.55 (m)	4.21 (d, 10.4)	3.56 (m)	4.22 (d, 10.3)	3.56 (m)	4.21 (m)
26	1.59 (m)	1.63 (m)	1.60 (m)	1.62 (m)	1.60 (m)	1.61 (m)
27	3.18 (t, 9.8)	3.55 (m)	3.20 (t, 9.8)	3.56 (m)	3.17 (m)	3.56 (m)
28	2.42 (m)	2.64 (td, 3.5, 10.0)	2.47 (m)	2.65 (td, 3.5, 10.2)	2.42 (m)	2.61 (m)
29	6.62 (d, 10.7)	6.79 (d, 10.1)	6.61 (d, 11.3)	6.80 (d, 10.0)	6.62 (d, 10.7)	6.78 (d, 10.1)
30	2.08 (s)	2.08 (s)	4.34/4.33 (s)	4.34/4.33 (s)	2.08 (s)	2.08 (s)
31	1.02 (s)	1.02 (s)	1.03 (d, 7.0)	1.03 (d, 7.0)	1.02 (s)	1.02 (s)
32	1.00 (s)	1.00 (s)	1.01 (d, 7.1)	1.01 (d, 7.1)	1.00 (s)	1.00 (s)
33	0.98 (s)	0.98 (s)	0.98 (d, 6.7)	0.98 (d, 6.7)	0.98 (s)	0.98 (s)
34	0.96 (s)	0.96 (s)	0.97 (d, 6.9)	0.97 (d, 6.9)	0.96 (s)	0.96 (s)
34a	4.54 (d, 8.4)	5.08 (d, 3.2)	4.56 (d, 6.9)	5.09 (d, 3.3)	4.54 (d, 6.9)	5.08 (d, 3.3)

* s: singlet, d: doublet, dd: double doublet, t: triplet, m: multiplet.

Table 2. ^{13}C NMR spectroscopic data (100 MHz, CD$_3$OD) of compounds **1**–**7** (δ_C) *.

| Position | 1 | | 2 | | 3 | | 4 | 5 | 6 | 7 |
	1a	1b	2a	2b	3a	3b				
1	184.7s	184.7s	184.1s	184.1s	184.1s	184.1s	183.7s	184.1s	184.0s	184.7s
2	143.0s	143.0s	143.2s	143.2s	142.4s	142.4s	142.7s	142.4s	142.4s	143.0s
3	117.3d	117.3d	117.2d	117.2d	117.2d	117.2d	117.2d	118.6d	119.1d	119.2d
4	187.1s	187.1s	186.8s	186.8s	186.5s	186.5s	186.8s	186.6s	186.9s	187.5s
5	103.7d	103.7d	108.6d	108.6d	108.8d	108.8d	108.9d	108.3s	108.1s	108.7s
6	165.9s	165.9s	163.9s	163.9s	164.0s	164.0s	164.0s	161.8s	163.6s	163.1s
MeO-6	57.0q	57.0q								
7	120.3s	120.3s	118.2s	118.2s	118.3s	118.3s	118.4s	119.2s	119.3s	119.2s
8	161.7s	161.7s	165.0s	165.0s	165.2s	165.2s	165.6s	164.0s	164.0s	164.7s
9	131.7s	131.7s	130.6s	130.6s	131.1s	131.1s	126.1s	125.5s	124.7s	126.0s
10	132.6s	132.6s	132.3s	132.3s	132.4s	132.4s	132.4s	129.9s	130.8s	130.9s
11	172.3s	172.3s	171.8s	171.8s	172.3s	172.3s	173.0s	200.1s	200.3s	201.1s
12	133.3s	132.4s	133.1s	131.5s	132.4s	131.1s	131.8s	141.6s	142.0s	142.0s
13	13.9q	13.3q	13.9q	13.3q	13.9q	13.3q	13.9q	12.7q	13.0q	13.4q
14	8.3q	8.3q	8.2q	8.2q	8.2q	8.2q	8.1q	8.7q	8.7q	9.3q
15	170.0s	170.0s	169.0s	169.0s	170.0s	170.0s	170.1s	172.2s	172.8s	172.2s
16	129.3s	129.3s	142.6s	142.6s	129.4s	129.4s	129.5s	132.2s	133.1s	133.4s
17	139.0d	139.0d	143.7d	143.7d	139.1d	139.1d	138.9d	135.2d	133.4d	136.2d
18	127.6d	127.6d	128.1d	128.1d	127.8d	127.8d	127.6d	126.3d	127.3d	136.2d
19	146.3d	146.3d	150.1d	150.1d	146.4d	146.4d	146.5d	141.6d	140.7d	126.1d
20	42.5d	42.5d	42.7d	42.7d	42.5d	42.5d	42.5d	39.2d	43.4d	77.0s
21	75.8d	75.8d	75.8d	75.8d	75.8d	75.8d	75.8d	74.9d	78.3d	76.7d
22	36.6d	36.6d	36.7d	36.7d	36.5d	36.5d	36.9d	34.4d	49.7d	35.3d
23	78.5d	78.5d	78.5d	78.5d	78.5d	78.5d	79.3 d	79.0d	211.3s	80.8d

Table 2. *Cont.*

Position	1		2		3		4	5	6	7
	1a	1b	2a	2b	3a	3b				
24	37.0d	37.0d	37.1d	37.1d	37.0d	37.0d	36.7d	38.0d	49.9d	39.0d
25	73.4d	72.8d	73.3d	72.8d	73.4d	72.7d	73.3d	71.3d	71.2d	72.3d
26	40.3d	41.3d	40.3d	41.3d	40.4d	41.3d	40.9d	43.9d	42.7d	44.6d
27	77.5d	73.4d	77.1d	73.3d	77.1d	73.4d	72.1d	68.7d	68.3d	70.0d
28	53.9d	50.7d	53.9d	50.7d	53.9d	50.7d	47.0d	46.1d	49.3d	49.1d
29	141.0d	142.4d	141.2d	142.7d	141.1d	142.4d	142.7d	139.0d	140.2d	141.5d
30	20.7q	20.7q	66.0t	66.0t	20.7q	20.7q	20.7q	20.3q	20.4q	21.0q
31	17.3q	17.3q	17.2q	17.2q	17.2q	17.2q	17.5q	18.2q	20.2q	26.7q
32	11.2q	11.2q	11.2q	11.2q	11.2q	11.2q	10.5q	11.3q	14.8q	14.6q
33	10.5q	10.5q	10.7q	10.7q	10.9q	10.9q	10.7q	8.9q	8.4q	9.8q
34	12.9q	12.9q	12.8q	12.8q	12.8q	12.8q	10.8q	11.8q	11.9q	12.4q
34a	98.2d	94.5d	98.0d	94.6d	98.0d	94.5d	64.6t	65.8t	64.4t	65.1t
AcO-34a								21.0q		
								172.9s		

* s: quaternary carbon, d: tertiary carbon, t: secondary carbon, q: primary carbon.

Table 3. ^{1}H NMR spectroscopic data (400 MHz, CD$_3$OD) of compounds **4–7** (δ_H, J in Hz) *.

Position	4	5	6	7
3	7.65 (s)	7.57 (s)	7.56 (s)	7.57 (s)
5	7.07 (s)			
13	1.89 (s)	2.08 (s)	2.04 (s)	2.06 (d, 1.0)
14	2.12 (s)	2.18 (s)	2.17 (s)	2.17 (s)
17	6.53 (t, 14.3)	6.25 (d, 10.8)	6.24 (d, 10.8)	6.26 (dd, 0.8, 10.9)
18	6.84 (dd, 10.9, 14.3)	6.51 (dd, 11.0, 15.8)	6.09 (dd, 11.0, 15.1)	5.96 (d, 16.0)
19	6.08 (dd, 8.2, 15.0)	6.09 (dd, 6.6, 15.9)	5.85 (dd, 9.6, 15.2)	6.47 (dd, 10.9, 15.9)
20	2.45 (m)	2.36 (m)	1.89 (m)	
21	3.82 (d, 8.8)	4.03 (m)	3.61 (dd, 1.5, 9.2)	3.95 (d, 1.2)
22	1.90 (m)	1.87 (m)	2.86 (dd, 6.8, 9.2)	2.01 (m)
23	3.60 (m)	3.48 (d, 10.2)		3.42 (q, 2.7, 9.4)
24	1.84 (m)	1.80 (m)	2.52 (m)	1.72 (m)
25	4.05 (d, 9.7)	3.98 (m)	3.87 (d, 10.2)	3.94 (dd, 1.9, 10.6)
26	1.80 (m)	1.43 (m)	1.35 (m)	1.40 (m)
27	4.13 (d, 5.5)	4.31 (s)	4.43 (s)	4.37 (br s)
28	2.82 (m)	2.89 (m)	2.58 (m)	2.65 (q, 7.1, 16.0)
29	6.91 (d, 10.4)	6.30 (d, 9.3)	6.28 (d, 9.1)	6.35 (dd, 1.0, 9.5)
30	2.09 (s)	2.09 (s)	2.05 (s)	2.10 (s)
31	1.00 (d, 6.8)	0.91 (d, 6.9)	1.06 (d, 3.1)	1.21 (s)
32	0.90 (d, 6.8)	1.05 (d, 7.0)	1.05 (d, 3.2)	1.17 (d, 7.0)
33	0.96 (d, 6.8)	0.72 (d, 6.8)	1.12 (d, 7.4)	0.74 (d, 6.8)
34	0.83 (d, 6.8)	0.40 (d, 7.0)	0.41 (d, 7.0)	0.41 (d, 7.0)
34a	3.62 (m)	4.01 (m)	3.52 (dd, 8.6, 10.9)	3.40 (m)
	3.54 (m)	4.00 (m)	3.38 (dd, 6.1, 11.0)	3.58 (dd, 8.0, 10.9)
AcO-34a		2.03 (s)		

* s: singlet, d: doublet, dd: double doublet, t: triplet, m: multiplet.

2.5. Bioactivity

2.5.1. Antimicrobial Assay

Compounds **1–13** were assayed for their antimicrobial activity against *Staphylococcus aureus* ATCC 25923, *Mycobacterium smegmatis* mc^2 155, *Pseudomonas aeruginosa* PA01 and *Proteusbacillus vulgaris* CPCC 160013 with the paper disk diffusion assay as previously described [21]. The tested compounds (20 μg/μL, 2 μL each) were absorbed onto individual paper disks (Ø 6 mm) and placed on the surface of the agar. The assay plates were incubated for 24 h at 37 °C and examined for the presence of inhibitory zones.

The MIC values of active compounds against the growth of *Staphylococcus aureus* ATCC 25923 were measured through the microbroth dilution method [22]. Microorganisms were cultured in LB media in 96-well plates at a concentration of 1×10^6 CFU/mL. The MIC values were obtained after incubating for 12 h at 37 °C with the tested compounds (concentration ranging from 320 to 0.039 µg/mL).

2.5.2. Cytotoxicity Assay

The in vitro antiproliferative activity against HeLa and Caco-2 cells was measured as previously reported [23,24]. Briefly, cells were seeded in 96-well plates at 7×10^3 cells/well and treated for 24 h with different concentrations of compounds **1–13**. Then, 10 µL Cell Counting Kit-8 (CCK-8) was added to each well and incubated for another 4 h. The absorbance was read at 480 nm by Spark 30086376 (TECAN, Männedorf, Switzerland).

3. Results

Compound **1** was determined to have the molecular formula $C_{36}H_{47}NO_{12}$ on the basis of the *quasi* molecular ion peaks at HRESIMS *m/z* 686.3172 [M + H]$^+$ (calcd for $C_{36}H_{48}NO_{12}{}^+$, 686.3171) and 708.2992 [M + Na]$^+$ (calcd for $C_{36}H_{48}NNaO_{12}{}^+$, 708.2990). The presence of a naphthaquinone chromophore was indicated by the HMBC correlations from H-3 (δ_H 7.64) to C-1 (δ_C 184.7), C-2 (δ_C 143.0) and C-10 (δ_C 132.6), and from H-14 (δ_H 2.09) to C-6 (δ_C 165.9), C-7 (δ_C 120.3) and C-8 (δ_C 161.7). The MeO-6 (δ_H 4.00) was supported by the HMBC correlations from MeO-6 to C-6 and NOE correlations from MeO-6 to H-5 (δ_H 7.18) (Tables 1 and 2, Tables S2 and S3, Figure 2). The twenty-four-carbon fragment from C-15 (δ_C 170.0) to C-11 (δ_C 172.3) was established on the basis of ^{1}H-^{1}H COSY correlations, along with the HMBC correlations from the H-30 (Me), H-31 (Me), H-32 (Me), H-33 (Me), H-34 (Me) and H-34a to the corresponding carbons (green, Figure 2). The hydroxylation of C-34a and oxidization to an aldehyde group followed by hemiacetal formation with the hydroxyl group at C-25 were determined based on the ^{1}H NMR of H-34a (δ_H 4.54/5.08) (Table 1, Figure 2). The *ansa* chain was determined to undergo retro-Claisen cleavage between C-5 and C-11 on the basis of the chemical shift of C-11 downfield, the presence of the extra aromatic proton H-5 compared to that of normal rifamycins and HMBC from H-5 to C-7 (Tables S2 and S3). Hence, the planar structure of **1** was established. The stereochemistry of the hemiacetal existed as a pair of epimers (**1a** and **1b**) at C-34a, and **1a** was determined to be α-form on the basis of the coupling constants $J_{34a,28} = 8.4$ Hz and the NOE correlations from H-34a (δ_H 4.54) to H-25 (δ_H 3.55) and H-27 (δ_H 3.18), and between H-25 and H-27. Accordingly, **1b** was determined to be β-form on the basis of the coupling constants $J_{34a,28} = 3.2$ Hz (Figure 2). The stereochemistry of other carbons was assumed to be the same as that of rifamycin W-hemiacetal [25] based on biosynthetic logic [12]. Thus, compound **1a** was named 34a-α-6-*O*-methyl-rifamycin W-M1-hemiacetal and **1b** was named 34a-β-6-*O*-methyl-rifamycin W-M1-hemiacetal.
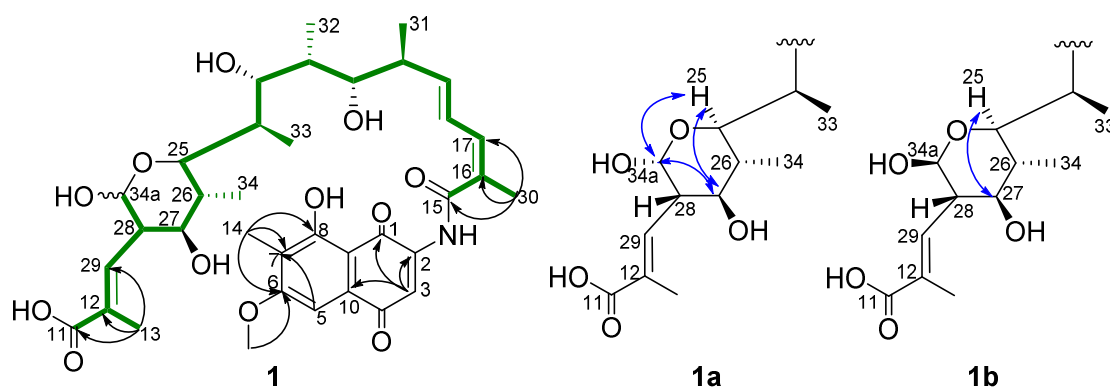
Figure 2. Selected HMBC (→), COSY (━) and NOESY (↔) correlations of **1**.

Compound **2** was confirmed to have the molecular formula $C_{35}H_{45}NO_{13}$ on the basis of the HRESIMS *quasi* molecular ion peaks at *m/z* 688.2956 [M + H]$^+$ and 710.2781 [M + Na]$^+$. The NMR spectroscopic data of **2** were similar to that of **1**, except that C-34 was a hydroxymethyl (δ_H 4.33, 4.34, δ_C 66.0) instead of a methyl group, and the 6-hydroxyl group was free (Tables 1 and 2). The relative configuration of **2** was proposed to be identical to that of **1**, and the hemiacetal existed as a pair of epimers (**2a** and **2b**) (Tables S4 and S5) as well. Thus, compound **2** was determined to be 34a-α-30-hydroxyrifamycin W-M1-hemiacetal (**2a**) and 34a-β-30-hydroxyrifamycin W-M1-hemiacetal (**2b**), respectively.

Similarly, the NMR (Tables S6 and S7) and HRESIMS (*m/z* 672.3011 [M + H]$^+$ and 694.2835 [M + Na]$^+$) comparison determined compound **3** to be 34a-α-rifamycin W-M1-hemiacetal (**3a**) and 34a-β-rifamycin W-M1-hemiacetal (**3b**), respectively.

The molecular formula of **4** was elucidated as $C_{35}H_{47}NO_{12}$ on the basis of the HRESIMS *quasi* molecular ion peaks at *m/z* 674.3172 [M + H]$^+$ and 696.2988 [M + Na]$^+$. Similar to that of compounds **1**, **2** and **3**, the *ansa* chain of **4** also underwent retro-Claisen cleavage between C-5 and C-11 due to the presence of the extra aromatic proton H-5 (δ_H 7.07), the chemical shift of C-11 (δ_C 173.0) and the HMBC from H-5 to C-7 (Tables 2 and 3, Table S8). Thus, compound **4** was determined to be rifamycin W-M1 [26].

The molecular formula of **5** was confirmed to be $C_{37}H_{47}NO_{12}$ by the HRESIMS *quasi* molecular ion peaks at *m/z* 698.3170 [M + H]$^+$ and 720.2986 [M + Na]$^+$. A close NMR comparison with that of rifamycin W (**12**) (Tables S9 and S12) [27] revealed that **5** was 34a-*O*-acetyl-rifamycin W, which was confirmed by the HMBC correlations between H-34a (δ_H 4.01, 4.00) and the acetyl carbon (δ_C 172.9).

The molecular formula of **6** was elucidated as $C_{35}H_{43}NO_{11}$ on the basis of the HRESIMS *quasi* molecular ion peaks at *m/z* 654.2914 [M + H]$^+$ and 676.2731 [M + Na]$^+$. NMR comparison with rifamycin W (**12**) (Tables S10 and S12) revealed that **6** was 23-ketorifamycin W on the basis of the downfield chemical shifts of C-22 (δ_C 49.7), C-23 (δ_C 211.3) and C-24 (δ_C 49.9).

Compound **7** was determined to have the molecular formula of $C_{35}H_{45}NO_{12}$ on the basis of HRESIMS *quasi* molecular ion peaks at *m/z* 672.3019 [M + H]$^+$ and 694.2839 [M + Na]$^+$, revealing one more oxygen atom than that of rifamycin W. NMR comparison (Tables S11 and S12) determined **7** to be 20-hydroxyrifamycin W, which was supported by the chemical shift of C-30 (δ_C 77.0).

Based on the 1D and 2D NMR data, HRESIMS data and spectroscopic comparisons with those reported in the literature, compounds **8–13** were determined to be rifamycin Z (**8**) [28], 30-hydroxyrifamycin W-hemiacetal (**9**) [29], rifamycin W-hemiacetal (**10**) [25,30], 30-hydroxyrifamycin W (**11**) [30], rifamycin W (**12**) [25,27] and protorifamycin I (**13**) [31] (Figure S7).

Compounds **1**−**13** were assayed for their antimicrobial activity against *Staphylococcus aureus* ATCC 25923, *Mycobacterium smegmatis* mc^2 155, *Pseudomonas aeruginosa* PA01 and *Proteusbacillus vulgaris* CPCC 160013. The results showed that new compounds **1–3** and known compounds **11** and **13** exhibited inhibitory activity against *S. aureus* ATCC 25923, while other compounds showed no antimicrobial activity (Figure S56). Thus, new compounds **1–3** were further tested for their antibacterial activity against *S. aureus* ATCC 25923 using the microbroth dilution method [22], and their MIC values were determined to be 5, 40 and 0.5 µg/mL, respectively (Table S14).

In view of no evident bactericidal activity, compounds **1–13** were evaluated for their antiproliferative activity against HeLa and Caco-2 cells using Cell Counting Kit-8 (CCK-8) (Bimake, Houston, TX, USA) and etoposide (VP-16) as a positive control. Compounds **1** and **3** showed modest activity in inhibiting the proliferation of HeLa and Caco-2 cells with IC$_{50}$ values of about 50 µM (Table S15, Figures S57 and S58).

4. Discussion

Post-PKS modifications play an important role in increasing the structural diversity and improving the biological activity of rifamycins. As the proposed earliest macrocyclic

intermediate in rifamycin post-PKS biosynthesis, proansamycin X tended to undergo dehydration to form putative protorifamycins (without C-8 hydroxyl group) or undergo dehydrogenation to form rifamycin W [24,32,33]. Rifamycin W undergoes a rearrangement of the polyketide backbone to produce rifamycin B via the oxidative cleavage of the C-12/C-29 double bond. The mechanism of this oxidative cleavage has not been characterized yet. For the *rif-orf5* gene, when cloned and heterologously expressed in *E. coli*, the recombinant protein showed spectra typical of P450 cytochromes [34]. Thus, the *rif-orf5* gene was confirmed to code for a cytochrome P450 enzyme, which is the key step for oxygen incorporation in rifamycin B biosynthesis and may be involved in the cleavage of the olefinic moiety of rifamycin W [16,17].

In this study, systematic isolation of the fermentation products of the mutant strain Δ*rif-orf5* afforded thirteen rifamycin W derivatives besides the main product rifamycin W (**12**), indicating that the *rif-orf5* gene was probably involved in the oxidative cleavage of the C-12/C-29 double bond. Compounds **1**–**4** all undergo C-5/C-11 retro-Claisen cleavage, as observed in the biosynthesis of proansamycin B-M1 and protorifamycin I–M1 [24,35], hygrocins I and J [36], divergolides R and S [37] and microansamycins G–I [38]. This C-5/C-11 cleavage probably occurred due to an over-accumulation of rifamycin W, which serves as a detoxification mechanism. Compounds **1**–**3**, **9** and **10** featured a hemiacetal, in which **9** and **10** existed in β-form according to the chemical shift of C-34a and the coupling constants between C-34a and C-28, while **1**–**3** existed as epimer pairs (Table S13), which may be due to the feasibility of polyketide chain cleavage in C-5/C-11. Additionally, the hemiacetal containing compounds **1**–**3**, **9** and **10**, as well as the lactone-containing rifamycin Z (**8**), indicated that the oxidation of C-34a alcohol to the carboxyl group may occur before the C-12/C-29 olefinic bond cleavage. In addition, compared to 8-deoxy rifamycins [24], compounds **5**, **6**, **7** and **11** also oxygenated at C-34a, C-23, C-20 and C-30, which suggested that the rifamycin *ansa* chain is prone to oxidization in these specific sites during fermentation (Figure 3).
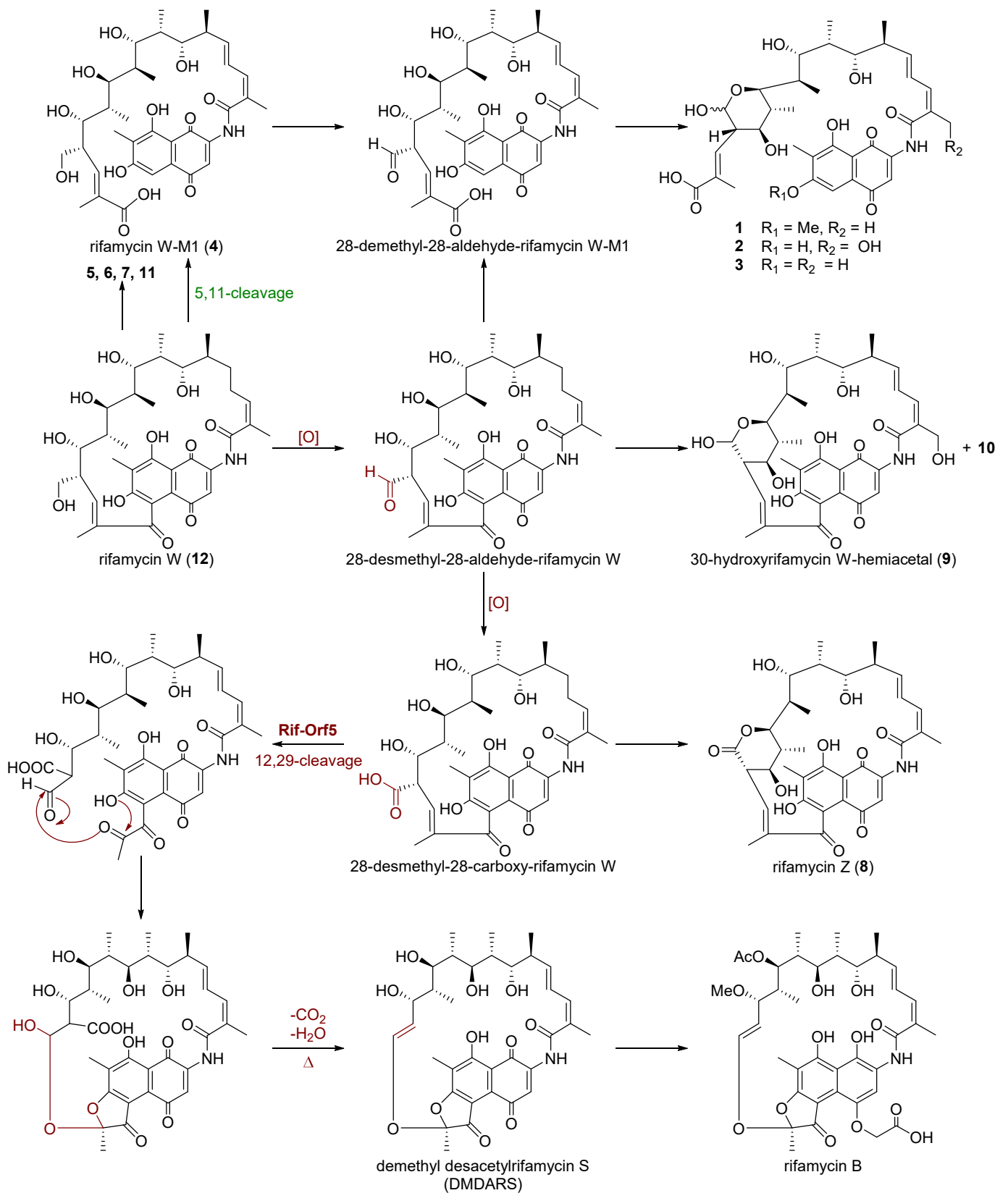
Figure 3. Proposed biosynthetic pathway of compounds from mutant Δ*rif-orf5*.

5. Conclusions

In this study, the cytochrome P450 monooxygenase gene *rif-orf5* was confirmed to be involved in the oxidative cleavage of the *ansa* chain of rifamycin W through in vivo gene inactivation and isolation of the main product rifamycin W. Systematic isolation of the fermentation products of the mutant strain Δ*rif-orf5* afforded seven new rifamycin W congeners, from which **1**–**3** featured two epimeric forms of hemiacetal at C-34a, and C-5/C-11 retro-Claisen cleavage. Compounds **1**–**3** exhibited antibacterial activity against *Staphylococcus aureus*, and **1** and **3** showed modest antiproliferative activity against HeLa and Caco-2 cells.

Supplementary Materials: The following are available online at https://www.mdpi.com/article/10.3390/biom11070920/s1, Figure S1: Construction flow chart for *rif-orf5* gene knock-out mutant Δ*rif-orf5*; Figure S2: Construction and enzymatic digestion verification of pOJ260-orf5, which was verified by sequencing; Figure S3: PCR verification of *rif-orf5* gene knock-out mutant Δ*rif-orf5*; Figure S4: Construction and enzymatic digestion verification of pSET152-orf5, which was verified by sequencing; Figure S5: PCR verification of *rif-orf5* gene complementation mutant Δ*rif-orf5::orf5*; Figure S6: HPLC detection of *rif-orf5* gene knock-out and gene complementation mutants; Figure S7: Structures of known compounds; Figure S8–S14: NMR and HRESIMS spectra of **1**; Figure S15–S21: NMR and HRESIMS spectra of **2**; Figure S22–S28: NMR and HRESIMS spectra of **3**; Figure S29–S34: NMR and HRESIMS spectra of **4**; Figure S35–S41: NMR and HRESIMS spectra of **5**; Figure S42–S48: NMR and HRESIMS spectra of **6**; Figure S49–S55: NMR and HRESIMS spectra of **7**; Figure S56: Antimicrobial activity of compounds **1**–**13**; Figure S57: Antiproliferative activity of compounds **1**–**13** (50 and 10 μM, respectively) against HeLa cells; Figure S58: Antiproliferative activity of compounds **1**–**13** (50 and 10 μM, respectively) against Caco-2 cells; Table S1: Primers used in this study; Table S2–S11: NMR data of compounds **1**–**7**; Table S12: NMR spectroscopic data for rifamycin W (**12**); Table S13: Selected ^{1}H NMR spectroscopic data for hemiacetal of compounds **1**–**3** and **9**, **10**; Table S14: Diameter of the inhibition zones and MIC of active compounds **1**–**3** against *Staphylococcus aureus* ATCC 25923; Table S15: Antiproliferative activity against HeLa and Caco-2 cells of compounds **1**–**13**.

Author Contributions: Conceptualization, Y.S. (Yuemao Shen); methodology, Y.S. (Yanrong Shi); formal analysis, Y.S. (Yanrong Shi); investigation, Y.S. (Yanrong Shi), F.Y., Y.S. (Yuliang Song) and X.Z.; data curation, Y.S. (Yanrong Shi) and F.Y.; writing—original draft preparation, Y.S. (Yanrong Shi); writing—review and editing, C.L. and Y.S. (Yuemao Shen); supervision, C.L. and Y.S. (Yuemao Shen); project administration, Y.S. (Yuemao Shen); funding acquisition, C.L. and Y.S. (Yuemao Shen). All authors have read and agreed to the published version of the manuscript.

Institutional Review Board Statement: Not applicable.

Informed Consent Statement: Not applicable.

Data Availability Statement: Not applicable.

Conflicts of Interest: The authors declare no conflict of interest. The funders had no role in the design of the study; in the collection, analyses, or interpretation of data; in the writing of the manuscript, or in the decision to publish the results.

References

1. Rinehart, K.L.; Shield, L.S. Chemistry of the ansamycin antibiotics. In *Fortschritte der Chemie Organischer Naturstoffe/Progress in the Chemistry of Organic Natural Products*; Herz, W., Grisebach, H., Kirby, G.W., Eds.; Springer: Vienna, Austria, 1976; Volume 33, pp. 231–307.
2. Wehrli, W. ChemInform Abstract: Ansamycins: Chemistry, biosynthesis and biological activity. *Chem. Inf.* **1978**, *9*, 21–49. [CrossRef]

3.   Sensi, P. Applications of paper chromatography & countercurrent distribution to steroids & antibiotics. *Boll. Chim. Farm.* **1957**, *96*, 437–457. [PubMed]

4.   Sensi, P.; Greco, A.M.; Gallo, G.G.; Rolland, G. Isolation and structure determination of a new amicetin-like antibiotic: Amicetin B. *Antibiot. Chemother.* **1957**, *7*, 645–652.

5.   Sensi, P.; Margalith, P.; Timbal, M.T. Rifomycin, a new antibiotic. Preliminary report. *Farmaco Sci.* **1959**, *14*, 146–147.

6.   Wehrli, W.; Staehelin, M. The rifamycins—Relation of chemical structure and action on RNA polymerase. *Biochim. et Biophys. Acta (BBA) Nucleic Acids Protein Synth.* **1969**, *182*, 24–29. [CrossRef]

7.   Ramos-e-Silva, M.; Rebello, P.F. Leprosy. Recognition and treatment. *Am. J. Clin. Dermatol.* **2001**, *2*, 203–211. [CrossRef]

8.   Murphy, C.K.; Karginova, E.; Sahm, D.; Rothstein, D.M. In Vitro Activity of Novel Rifamycins against Gram-positive Clinical Isolates. *J. Antibiot.* **2007**, *60*, 572–576. [CrossRef]

9.   Czerwonka, D.; Domagalska, J.; Pyta, K.; Kubicka, M.M.; Pecyna, P.; Gajecka, M.; Przybylski, P. Structure–activity relationship studies of new rifamycins containing (L) -amino acid esters as inhibitors of bacterial RNA polymerases. *Eur. J. Med. Chem.* **2016**, *116*, 216–221. [CrossRef]

10. Girling, D.J. Adverse reactions to rifampicin in antituberculosis regimens. *J. Antimicrob. Chemother.* **1977**, *3*, 115–132. [CrossRef]

11. Goldstein, B.P. Resistance to rifampicin: A review. *J. Antibiot.* **2014**, *67*, 625–630. [CrossRef]

12. August, P.R.; Tang, L.; Yoon, Y.J.; Ning, S.; Müller, R.; Yu, T.-W.; Taylor, M.; Hoffmann, D.; Kim, C.-G.; Zhang, X.; et al. Biosynthesis of the ansamycin antibiotic rifamycin: Deductions from the molecular analysis of the rif biosynthetic gene cluster of *Amycolatopsis mediterranei* S699. *Chem. Biol.* **1998**, *5*, 69–79. [CrossRef]

13. Li, T.; Yoon, Y.J.; Choi, C.-Y.; Hutchinson, C.R. Characterization of the enzymatic domains of in the modular polyketide synthase involved in rifamycin B biosynthesis by *Amycolatopsis mediterranei*. *Gene* **1998**, *216*, 255–265. [CrossRef]

14. Schupp, T.; Toupet, C.; Engel, N.; Goff, S. Cloning and sequence analysis of the putative rifamycin polyketide synthase gene cluster from *Amycolatopsis mediterranei*. *FEMS Microbiol. Lett.* **1998**, *159*, 201–207. [CrossRef]

15. Floss, H.G.; Yu, T.-W. Lessons from the rifamycin biosynthetic gene cluster. *Curr. Opin. Chem. Biol.* **1999**, *3*, 592–597. [CrossRef]

16. Floss, H.G.; Yu, T.-W. Rifamycin-Mode of Action, Resistance, and Biosynthesis. *Chem. Rev.* **2005**, *105*, 621–632. [CrossRef]

17. Xu, J.; Wan, E.; Kim, C.-J.; Floss, H.G.; Mahmud, T. Identification of tailoring genes involved in the modification of the polyketide backbone of rifamycin B by *Amycolatopsis mediterranei* S699. *Microbiology* **2005**, *151*, 2515–2528. [CrossRef] [PubMed]

18. Bierman, M.; Logan, R.; O'Brien, K.; Seno, E.; Rao, R.N.; Schoner, B. Plasmid cloning vectors for the conjugal transfer of DNA from *Escherichia coli* to *Streptomyces* spp. *Gene* **1992**, *116*, 43–49. [CrossRef]

19. Hu, Z.; Hunziker, D.; Hutchinson, C.R.; Khosla, C. A host–vector system for analysis and manipulation of rifamycin polyketide biosynthesis in *Amycolatopsis mediterranei*. *Microbiology* **1999**, *145*, 2335–2341. [CrossRef]

20. Gibson, D.G.; Young, L.; Chuang, R.Y.; Venter, J.C.; Hutchison, C.A., 3rd; Smith, H.O. Enzymatic assembly of DNA molecules up to several hundred kilobases. *Nat. Methods* **2009**, *6*, 343–345. [CrossRef] [PubMed]

21. Raahave, D. Paper Disk-Agar Diffusion Assay of Penicillin in the Presence of Streptomycin. *Antimicrob. Agents Chemother.* **1974**, *6*, 603–605. [CrossRef] [PubMed]

22. Arendrup, M.C.; Prakash, A.; Meletiadis, J.; Sharma, C.; Chowdhary, A. Comparison of EUCAST and CLSI reference microdilution MICs of eight antifungal compounds for Candida auris and associated tentative epidemiological cutoff values. *Antimicrob. Agents Chemother.* **2017**, *61*, e00485-17. [CrossRef]

23. Jiang, Z.; Zhou, Q.; Ge, C.; Yang, J.; Li, H.; Chen, T.; Xie, H.; Cui, Y.; Shao, M.; Li, J.; et al. Rpn10 promotes tumor progression by regulating hypoxia-inducible factor 1 alpha through the PTEN/Akt signaling pathway in hepatocellular carcinoma. *Cancer Lett.* **2019**, *447*, 1–11. [CrossRef] [PubMed]

24. Ye, F.; Shi, Y.; Zhao, S.; Li, Z.; Wang, H.; Lu, C.; Shen, Y. 8-Deoxy-rifamycin derivatives from *Amycolatopsis mediterranei* S699 Δ*rifT* strain. *Biomolecules* **2020**, *10*, 1265. [CrossRef] [PubMed]

25. Stratmann, A.; Schupp, T.; Toupet, C.; Schilling, W.; Oberer, L.; Traber, R. New Insights into Rifamycin B Biosynthesis: Isolation of Proansamycin B and 34a-Deoxy-rifamycin W as Early Macrocyclic Intermediates Indicating Two Separated Biosynthetic Pathways. *J. Antibiot.* **2002**, *55*, 396–406. [CrossRef]

26. Ghisalba, O.; Traxler, P.; Fuhrer, H.; Richter, W.J. Early intermediates in the biosynthesis of ansamycins. III. Isolation and identification of further 8-deoxyansamycins of the rifamycin-type. *J. Antibiot.* **1980**, *33*, 847–856. [CrossRef]

27. Richard, J.W.; Edoardo, M.; Giancarlo, L. Ansamycin biogenesis: Studies on a novel rifamycin isolated from a mutant strain of *Nocardia mediterranei*. *Proc. Natl. Acad. Sci. USA* **1974**, *71*, 3260–3264. [CrossRef]

28. Cricchio, R.; Antonini, P.; Ferrari, P.; Ripamonti, A.; Tuan, G.; Martinelli, E. Rifamycin Z, a novel ansamycin from a mutant of *Nocardia mediterranea*. *J. Antibiot.* **1981**, *34*, 1257–1260. [CrossRef]

29. Shi, Y.; Zhang, J.; Tian, X.; Wu, X.; Li, T.; Lu, C.; Shen, Y. Isolation of 11,12-seco-Rifamycin W Derivatives Reveals a Cleavage Pattern of the Rifamycin Ansa Chain. *Org. Lett.* **2019**, *21*, 900–903. [CrossRef] [PubMed]

30. Traxler, P.; Schupp, T.; Fuhrer, H.; Richter, W.J. 3-Hydroxyrifamycin S and further novel ansamycins from a recombinant strain R-21 of *Nocardia mediterranei*. *J. Antibiot.* **1981**, *34*, 971–979. [CrossRef] [PubMed]

31. Ghisalba, O.; Traxler, P.; Nuesch, J. Early intermediates in the biosynthesis of ansamycins. I. Isolation and identification of protorifamycin I. *J. Antibiot.* **1978**, *31*, 1124–1131. [CrossRef]

32. Stratmann, A.; Toupet, C.; Schilling, W.; Traber, R.; Oberer, L.; Schupp, T. Intermediates of rifamycin polyketide synthase produced by an *Amycolatopsis mediterranei* mutant with inactivated *rifF* gene. *Microbiology* **1999**, *145*, 3365–3375. [CrossRef] [PubMed]

33. Yu, T.-W.; Shen, Y.; Doi-Katayama, Y.; Tang, L.; Park, C.; Moore, B.; Hutchinson, C.R.; Floss, H.G. Direct evidence that the rifamycin polyketide synthase assembles polyketide chains processively. *Proc. Natl. Acad. Sci. USA* **1999**, *96*, 9051–9056. [CrossRef]

34. Mejía, A.; Luna, D.; Fernández, F.J.; Barrios-González, J.; Gutierrez, L.H.; Reyes, A.G.; Absalón, A.E.; Kelly, S. Improving rifamycin production in *Amycolatopsis mediterranei* by expressing a Vitreoscilla hemoglobin (vhb) gene fused to a cytochrome P450 monooxygenase domain. *3 Biotech* **2018**, *8*, 456. [CrossRef] [PubMed]

35. Ghisalba, O.; Traxler, P.; Fuhrer, H.; Richter, W.J. Early intermediates in the biosynthesis of ansamycins. II. Isolation and identification of proansamycin B-M1 and protorifamycin I-M1. *J. Antibiot.* **1979**, *32*, 1267–1272. [CrossRef] [PubMed]

36. Li, S.; Lu, C.; Ou, J.; Deng, J.; Shen, Y. Overexpression of hgc1 increases the production and diversity of hygrocins in *Streptomyces* sp. LZ35. *RSC Adv.* **2015**, *5*, 83843–83846. [CrossRef]

37. Zhao, G.; Li, S.; Guo, Z.; Sun, M.; Lu, C. Overexpression of div8 increases the production and diversity of divergolides in *Streptomyces* sp. W112. *RSC Adv.* **2015**, *5*, 98209–98214. [CrossRef]

38. Wang, J.; Li, W.; Wang, H.; Lu, C. Pentaketide Ansamycin Microansamycins A–I from Micromonospora sp. Reveal Diverse Post-PKS Modifications. *Org. Lett.* **2018**, *20*, 1058–1061. [CrossRef] [PubMed]